

# Spontaneous formation of vortices and gray solitons in a spinor polariton fluid under coherent driving

S. S. Gavrilov

*Institute of Solid State Physics RAS, 142432 Chernogolovka, Russia;**Faculty of Physics, National Research University Higher School of Economics, 101000 Moscow, Russia;**and A. M. Prokhorov General Physics Institute RAS, 119991 Moscow, Russia*

(Received 24 September 2019; revised 22 August 2020; accepted 25 August 2020; published 23 September 2020)

It is generally accepted that quantized vortices formed in coherent bosonic fluids are “excitations” and as such do not arise in a one-mode condensate at zero temperature. To excite them, one needs either inhomogeneities (impurities, rotation, etc.) or essentially finite fluctuations. Here, we predict a perfectly spontaneous formation of vortices even at zero temperature, which takes place in a homogeneous cavity-polariton system under one-mode optical excitation at normal incidence. In spite of the absence of equilibrium and U(1) invariance, this system shows a counterpart of the Berezinskii-Kosterlitz-Thouless crossover between single vortices and coupled vortex-antivortex states ranging from small dipoles to rectilinear filaments with long-range ordering.

DOI: [10.1103/PhysRevB.102.104307](https://doi.org/10.1103/PhysRevB.102.104307)

## I. INTRODUCTION

Equilibrium Bose-Einstein condensates obey an autonomous U(1)-invariant wave equation, however, the very onset of macroscopic coherence is accompanied by symmetry breaking so that all particles share the same spontaneously chosen phase. When the symmetry is broken, the underlying phase freedom reveals itself in quantized vortices, topological excitations arising because of a weak pairwise repulsion of particles. Vortices were observed in various systems including quantum liquids [1,2], superconductors [3], cold atoms [4,5], and microcavities [6–8]. Here, we consider cavity polaritons, mixed states of photons and excitons formed in a thin layer of a semiconductor microcavity [9,10]. Their coherent states originate in two ways, (i) via Bose-Einstein condensation from a nonresonantly pumped excitonic reservoir to the ground state [11] or, owing to the photonic component, (ii) directly under resonant and coherent optical driving [12]. In contrast to equilibrium systems, a directly driven condensate displays forced oscillations and its phase is not free but imposed by the pump wave. For this reason all known ways to excite vortices resonantly involve artificial patterning of the incident pump beam and/or intracavity resonance energy [13–23]. In this study, we have found a different way of vortex formation that does not require any seeding inhomogeneities.

We report quantized vortices that originate specifically under the conditions of resonant excitation owing to spontaneous breakdown of the spin-reversal symmetry (parity). Parity and then a continuous spatial symmetry break down when opposite spin components of the field are linearly coupled, in addition to the usual pairwise repulsion of parallel spins. As a result, a perfectly uniform and spin-symmetric initial state of the system is divided into large-scale domains that differ in the way of symmetry breaking. Two equally possible steady

states have opposite phases, so they annihilate each other and the boundary between different domains is highly unstable, giving birth to vortices in a two-dimensional system and gray solitons in a one-dimensional system. In certain respects these excitations are similar to their equilibrium counterparts, for instance, vortex-antivortex dipoles and filaments arise in analogy to atomic gases [24–26], which is surprising, however, in view of the absence of thermal equilibrium in the driven system. The rotational symmetry is broken even for individual vortices; as a result, they interact on a large scale and form internally ordered structures. The spatial distribution of polarization around vortices is also uncommon and does not fit into the conventional row of the half- [8,27], full-, and spin-vortex states [20] or linear-polarization vortices [21,22].

Below, we describe the mean-field model (Sec. II), analyze its stationary solutions, and explain symmetry breakdown (Sec. III) that leads to the gray-soliton or vortex states (Sec. IV). Additional numerical examples, high-resolution images, and video files representing system dynamics are included in the Supplemental Material [28].

## II. MEAN-FIELD MODEL

Let us consider a planar polariton system excited at normal incidence by a coherent light wave. Polaritons have two spin states corresponding to right- and left-handed circular polarizations of light. Opposite spin states do not interact pairwise if the driven mode is far below the exciton level and the temperature is close to zero [29–32]. However, they can be linearly coupled owing to the lifted degeneracy of eigenstates with orthogonal polarizations, e.g., because of a mechanical stress [33–36]. This system is described by two mean-field amplitudes  $\psi_{\pm}(\mathbf{r}, t)$  obeying the “driven” Gross-Pitaevskii

equations [10]

$$i\hbar \frac{\partial \psi_{\pm}}{\partial t} = (\hat{E} - i\gamma + V\psi_{\pm}^* \psi_{\pm})\psi_{\pm} + \frac{g}{2}\psi_{\mp} + f_{\pm}e^{-iE_p t/\hbar}. \quad (1)$$

Here,  $\hat{E} = \hat{E}(-i\hbar\nabla)$  is the energy operator determined by the lower-polariton dispersion law  $E(k)$  that is nearly parabolic for small in-plane wave numbers  $k$ ;  $\gamma$  is the decay rate,  $V > 0$  is the polariton-polariton interaction constant, and  $g/2$  is the spin coupling rate. Amplitudes  $f_{\pm}$  are proportional to the respective polarization components of the external electric field. If  $f_{\pm} \rightarrow 0$  and  $\psi_{\pm} \rightarrow 0$ , the system is diagonalized by the unitary transformation  $\psi_{\pm} = (\psi_x \mp i\psi_y)/\sqrt{2}$ ; the eigenstates are orthogonally polarized and have energy levels  $E_{x,y}(k) = E(k) \pm g/2$ . The pump frequency  $E_p/\hbar$  is supposed to be close to the resonance frequencies of the driven polariton state with zero  $k$ .

### III. SYMMETRY BREAKDOWN

Throughout this paper we consider the case of  $x$ -polarized spin-symmetric excitation ( $f_+ = f_- = f$ ), so that the equations for  $\psi_+$  and  $\psi_-$  are exactly the same. They have one-mode solutions of the form  $\psi_{\pm}(t) = \bar{\psi}_{\pm}e^{-iE_p t/\hbar}$ . Amplitudes  $\bar{\psi}_{\pm}$  obey time-independent equations

$$(D + i\gamma - V|\bar{\psi}_{\pm}|^2)\bar{\psi}_{\pm} - \frac{g}{2}\bar{\psi}_{\mp} = f, \quad (2)$$

where  $D = E_p - E(k=0)$  is the pump detuning from the mean (unsplit) ground-state level. This system is multistable [37]. Clearly, it has spin-symmetric solutions with  $\bar{\psi}_+ = \bar{\psi}_-$  for each  $f$ , which we henceforth denote as the  $\Pi$  states. They are copolarized with the incident pump and feature intrinsic bistability when  $D - g/2 > \sqrt{3}\gamma$  [38,39].

To demonstrate different solutions, let us equate the left-hand sides of Eqs. (2), which yields

$$\frac{\bar{\psi}_-}{\bar{\psi}_+} = \frac{D + g/2 + i\gamma - V|\bar{\psi}_+|^2}{D + g/2 + i\gamma - V|\bar{\psi}_-|^2}. \quad (3)$$

If  $V|\bar{\psi}_{\pm}|^2 = D + g/2$ , then  $\bar{\psi}_{\mp} \propto \gamma$ , so that the circular-polarization degree (also referred to as the third Stokes parameter)  $S_3 = (|\bar{\psi}_+|^2 - |\bar{\psi}_-|^2)/(|\bar{\psi}_+|^2 + |\bar{\psi}_-|^2)$  nearly reaches  $\pm 1$  at small  $\gamma$ . This doublet of steady states will be denoted as  $\Sigma_{\pm}$ . Such states were experimentally observed in a microcavity with  $g \gtrsim \gamma$  [34–36].

Another way of parity breaking comes into play at greater  $g/\gamma$  and is directly responsible for vortices and gray solitons. Suppose  $V|\bar{\psi}_{\pm}|^2 = D + g/2 \pm \delta$ , so that Eq. (3) turns into

$$\frac{\bar{\psi}_-}{\bar{\psi}_+} = \frac{i\gamma - \delta}{i\gamma + \delta}. \quad (4)$$

Now one can express  $\bar{\psi}_-$  in terms of  $\bar{\psi}_+$  and substitute it in Eq. (2) for  $\bar{\psi}_+$ , which, after multiplication of both sides by the complex conjugate, leads to the following equation for  $\delta$ ,

$$\left(\gamma^2 + \delta^2 + \frac{\gamma^2 g^2}{\gamma^2 + \delta^2}\right)\left(D + \frac{g}{2} + \delta\right) = Vf^2. \quad (5)$$

If  $|\delta|$  is much smaller than  $g$  and  $D$ , one can drop  $\delta$  in the second parentheses of Eq. (5) which is thereby reduced to a

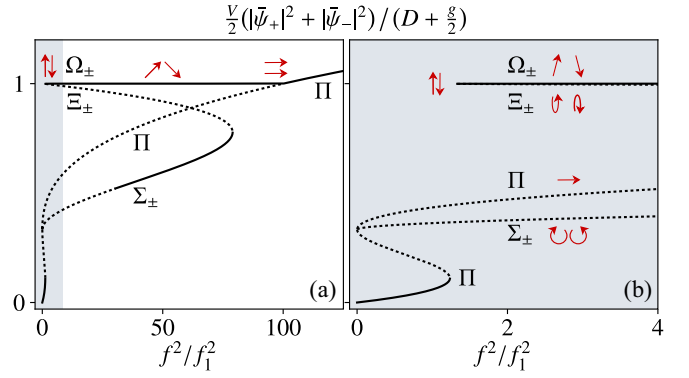


FIG. 1. One-mode response functions [solutions of Eq. (2)] at  $\gamma = 5 \mu\text{eV}$  and  $g = D = 1 \text{ meV}$ , so that  $f_2^2/f_1^2 = g/2\gamma = 100$ . Solutions shown by dotted lines are unstable even in the one-mode limit with  $k = 0$ . (b) shows a magnified interval of (a) at small  $f$  which will be mainly considered in this paper; arrows and ellipses schematically indicate polarization states.

quadratic equation for  $\gamma^2 + \delta^2$ . The latter has positive roots starting with pump intensity

$$f_1^2 = \frac{2\gamma g}{V}\left(D + \frac{g}{2}\right), \quad (6)$$

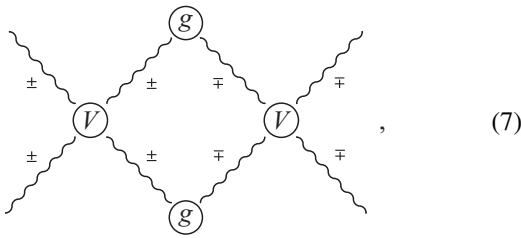
where the root *per se* is  $\gamma^2 + \delta^2 = \gamma g$ . The smallness of  $|\delta|$  is justified when  $\gamma \ll g \sim D$ , in which case the overall consideration based on Eq. (4) is self-consistent. Near the threshold point  $f = f_1$  we have  $\delta/g \rightarrow 0$  and  $\delta/\gamma \rightarrow \infty$  if  $\gamma/g \rightarrow 0$ . Then, in accordance with Eq. (4),  $\bar{\psi}_-/\bar{\psi}_+ \rightarrow -1$ , so that the condensate is polarized in the  $y$  direction (orthogonally to the pump).

Being very small at the threshold,  $|\delta|$  decreases still further with increasing  $f$  for one of two pairs of solutions of Eq. (5). At  $f \gg f_1$  and  $\gamma \ll g$  we have  $\delta(f) = \pm\gamma\sqrt{f_2^2/f^2 - 1}$ , where  $f_2^2 = (g/2\gamma)f_1^2$  is the upper threshold at which  $|\delta|$  eventually turns to zero. Below this point, the condensate has constant total intensity  $I = |\bar{\psi}_+|^2 + |\bar{\psi}_-|^2$  but varying polarization direction. The  $(x, y)$  polarization degree,  $S_1 = (|\bar{\psi}_x|^2 - |\bar{\psi}_y|^2)/I$ , shows a linear increase as a function of  $f^2$  and ranges from about  $-1$  at  $f = f_1$  to  $+1$  at  $f = f_2$ . The solutions with mutually opposite  $\delta$  differ in the sign of the “diagonal” linear polarization  $S_2 = (\bar{\psi}_x^* \bar{\psi}_y + \bar{\psi}_y^* \bar{\psi}_x)/I$ . Since the length of the Stokes vector  $(S_1, S_2, S_3)$  is unity and its circular-polarization component  $S_3 = \delta/(D + g/2)$  is negligible, we have  $S_2 \approx \pm\sqrt{1 - S_1^2}$  and, in particular,  $S_2 \approx \pm 1$  at  $f^2 = (f_1^2 + f_2^2)/2$ . Let us denote this doublet of solutions as  $\Omega_{\pm}$ . They appear at  $f = f_1$  and degenerate into the singlet  $\Pi$  branch at  $f = f_2$  (Fig. 1).

For a cousin doublet of solutions, henceforth  $\Xi_{\pm}$ , the value of  $|\delta|$  grows with  $f$ , so the field gradually acquires noticeable  $S_3$ . Since then ratio (4) does not satisfy Eq. (2) even approximately. As seen in Fig. 1, the intensity of the  $\Xi$  states decreases with increasing  $f$ , which is indicative of instability. Sooner or later the  $\Xi$  doublet meets the  $\Sigma$  doublet and they both terminate.

The  $\Omega$  doublet is the only possible type of steady states in a wide interval of  $f^2$  when  $\gamma \ll g \sim D$ . The instabilities of the  $\Pi$  and  $\Sigma_{\pm}$  states were investigated earlier, and here

we only briefly recall the main results. The spin-symmetric  $\Pi$  state is unstable because an indefinitely small imbalance of  $|\psi_+|$  and  $|\psi_-|$  makes the greater component grow further by simultaneously suppressing the minor one [34–36,40–42]. This occurs at  $g \gtrsim \gamma$  and leads to one of the  $\Sigma_{\pm}$  states. After one of the spin components has been suppressed, a significant increase in the pump intensity is required for driving it up again, so that the length of the  $\Sigma$  branches in a diagram such as Fig. 1 is quite great. Notice as well that the Josephson oscillations [43] are not possible when both spin components have the same “forced” frequency  $E_p/\hbar$  and thus their phase difference does not vary with time. In turn, the pairwise interaction conserves spin and, taken alone, it also cannot help restore spin symmetry. However, the  $\Sigma$  branches lose stability with respect to a higher-order interaction process,



which simultaneously enables spins to be reversed and lifts the frequency degeneracy. Namely, even when the condensate at  $k = 0$  and  $E = E_p$  has a perfectly circular polarization, new energy levels with different polarizations get populated at  $E \approx E_p \pm D$  in a finite interval of  $k$  around  $k = 0$ . This process starts at  $g \approx 4\gamma$  [40,44] and leaves no one-mode solutions within a certain range of  $f^2$ , which results in turbulence [45], periodic spin networks, and chimera states [46].

Given that  $g \sim D > 0$ , a decrease in  $\gamma$  broadens the interval of  $f^2$  in which the  $\Pi$  and  $\Sigma_{\pm}$  states are forbidden. At the same time, it lowers the critical point  $f_1^2 \propto \gamma$  where the  $\Omega_{\pm}$  states appear. They have the greatest intensity for each  $f_1 \leq f \leq f_2$  and are always stable.

The  $\Pi \rightarrow \Omega$  transition is markedly different from the  $\Pi \rightarrow \Sigma$  transition observed at  $g \sim \gamma$ . First, the superposition of  $\Omega_+$  and  $\Omega_-$  has extremely low intensity near  $f = f_1$ . To make it clear, notice that replacing  $\psi_+$  with  $\psi_-$  and vice versa turns  $\Omega_+$  into  $\Omega_-$  and  $\Sigma_+$  into  $\Sigma_-$  in view of symmetry. Thus, the average state for each doublet [e. g.,  $(\Omega_+ + \Omega_-)/2$ ] is spin symmetric and must have the  $x$  polarization direction in accordance with the usual definition  $\psi_{\pm} = (\psi_x \mp i\psi_y)/\sqrt{2}$ . We have found, however, that both  $\Omega_{\pm}$  states are nearly  $y$  polarized at  $f = f_1$ . To add up to an  $x$ -polarized state, they must have opposite phases and annihilate each other, which also applies to the  $\Xi_{\pm}$  pair. That is why a turnover point between  $\Omega_+$  and  $\Omega_-$  can behave as a gray soliton or vortex core.

Second, notice that the outcome of the  $\Pi \rightarrow \Sigma_{\pm}$  transition is determined in its very beginning by the sign of  $|\psi_+| - |\psi_-|$ . By contrast, the outcome of the  $\Sigma_{\pm} \rightarrow \Omega_{\pm}$  transition is uncertain at its early stage because processes (7) make a continuum of different  $k$  states populated concurrently [40,44]. Thus, after the spin symmetry breaking, the system loses homogeneity simultaneously at each point and goes through a stage of

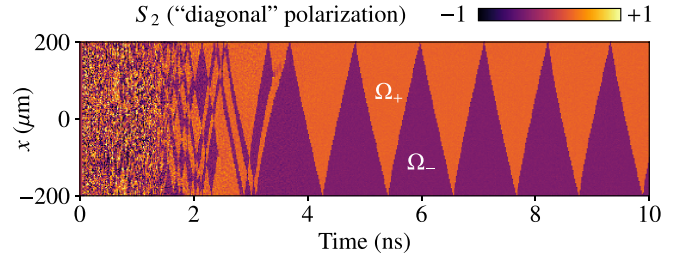


FIG. 2. Solution of Eq. (1) at  $\gamma = 1 \mu\text{eV}$ ,  $g = D = 1 \text{ meV}$ , and  $f^2/f_1^2 = 11$  in the one-dimensional case; the initial state is homogeneous (zero). The boundary between the  $\Omega_{\pm}$  states behaves as a gray soliton; it runs with a constant speed and gets reflected from the 2-meV high potential walls at  $x = \pm 200 \mu\text{m}$ .

strong spatiotemporal disorder. Different examples of spontaneous phenomena in driven polariton fluids (not involving vortices or spin) can be found in Refs. [47,48].

#### IV. VORTICES AND GRAY SOLITONS

The following numerical experiments are performed with typical parameters of a GaAs-based microcavity. The exciton-photon detuning at  $k = 0$  is zero, the full Rabi splitting is 10 meV, and the exciton mass is much greater than the photon mass  $\epsilon E/c^2$ , where  $\epsilon = 12.5$  and  $E = 1.5 \text{ eV}$ . The interaction constant  $V$  can be chosen arbitrarily, as it only determines a critical point (6). A small white-noise term is added to the right-hand side of Eq. (1) to simulate fluctuations. The pump is smoothly switched on during 0.1 ns and then held constant. The boundary conditions are set by means of a sharp increase in the polariton energy or decay rate. The case of a purely homogeneous system with periodic boundary conditions is discussed in the Supplemental Material [28].

Figure 2 shows a 400- $\mu\text{m}$ -long one-dimensional polariton system with potential walls near the boundaries. After the stage of disorder, it nearly approaches equilibrium but remains two-component. A pair of the  $\Omega_{\pm}$  domains are separated by a gray soliton, pointlike interface where total intensity  $I$  drops down. When  $\gamma/g$  is small and  $f$  close to  $f_1$ , such a soliton can endlessly run and even reflect from the potential walls. Colliding solitons cancel each other, thus, only one can survive in the long term, resulting in spatiotemporal self-pulsations seen in Fig. 2. Increasing  $f$  renders solitons motionless. Since the  $\Omega_{\pm}$  states do not annihilate each other completely when  $f$  is high, the interface between the two domains can be a plain superposition of  $\Omega_+$  and  $\Omega_-$  which is spin symmetric and static. However, at  $f = f_1$  such  $\Omega$ -symmetric states would have zero amplitude and become highly unstable; instead of that, solitons acquire a nonzero amplitude along with a certain degree of asymmetry and move in space.

The two-dimensional case is essentially more complex. Of particular interest is the boundary between the  $\Omega_{\pm}$  domains, its shape and polarization. To simplify our first example and skip the turbulent stage, we have used rotationally symmetric initial conditions biased to the  $\Omega_+$  and  $\Omega_-$  states, respectively, inside and outside a circle placed at the grid center. Accordingly, the pump was not “switched on” smoothly but had a fixed amplitude  $f$  at all  $t$ . Figure 3 shows the steady state

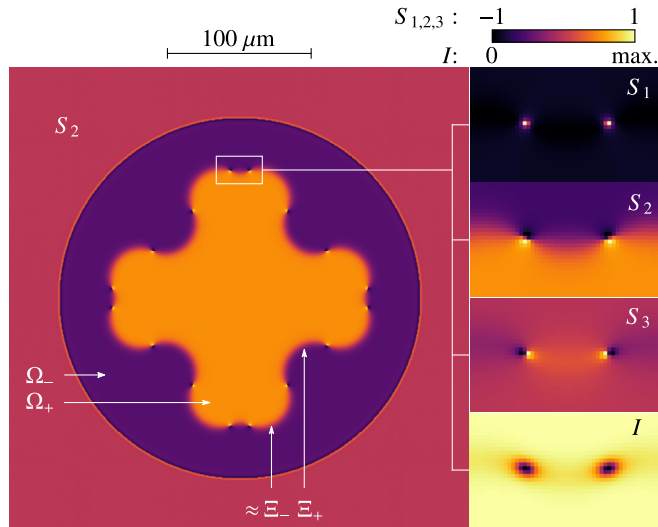


FIG. 3. Intensity  $I$  and polarization degrees (normalized Stokes parameters)  $S_{1,2,3}$  for a steady solution of Eq. (1) formed in about 1 ns at  $f^2/f_1^2 \approx 6.8$ . Parameters  $\gamma$ ,  $g$ , and  $D$  correspond to Fig. 1. The initial conditions were biased to the  $\Omega_+$  and  $\Omega_-$  states at  $|\mathbf{r}| \leq 20 \mu\text{m}$  and  $|\mathbf{r}| > 20 \mu\text{m}$ , respectively,  $r = 0$  being the grid center. To ensure zero boundary conditions,  $\gamma$  is increased up to 4 meV at  $|\mathbf{r}| = 125 \mu\text{m}$ . The insets show a magnified fragment with two vortices of opposite topological charge.

to which such a system came in about 1 ns. The borderline between the  $\Omega_+$  and  $\Omega_-$  domains comprises 16 curved segments whose polarizations appear to be very close to the  $\Xi$  states. Being not  $\Omega$  symmetric, the  $\Xi_{\pm}$ -state segments tend to move in opposite directions from  $\Omega_{\mp}$  to  $\Omega_{\pm}$ , thus, each turnover point between  $\Xi_+$  and  $\Xi_-$  carries a vortex core and has very low intensity. Neighboring vortices with opposite rotation directions balance each other and help stabilize the system.

The Stokes vector components shown in Fig. 3 allow one to deduce the phase distribution around the core. It is seen that  $S_3 \sim \pm 1$  and  $S_2 \sim \pm 1$ , respectively, along the tangent and the normal to the borderline. The signs of  $S_2$  and  $S_3$  match the  $\Omega_{\pm}$  domains and  $\Xi_{\pm}$  segments. A purely circular polarization  $S_3 = \pm 1$  implies that the  $(x, y)$  phase difference  $\Delta\phi = \arg(\psi_x^* \psi_y)$  is equal to  $\pi/2$  or  $3\pi/2$ , whereas  $S_2 = \pm 1$  implies  $\Delta\phi = 0$  or  $\pi$ . Thus,  $\Delta\phi$  makes an angle of  $\pm 2\pi$  around the core. At the same time, the orientation of the  $S_{2,3}$  poles is certain and reflects the long-range symmetry breaking.

When two vortices of opposite charge come within short distances of each other, the borderline segment enclosed between them becomes straight. Calculations show that many adjacent vortex-antivortex pairs may cancel their high- $S_3$  poles along the “core” line with  $S_1 = +1$  and align the  $S_2$  poles on both sides of that line, resulting in straight  $\Omega$ -symmetric filaments. At larger  $f/f_1$ , when such symmetric states have a noticeably nonzero amplitude and can be stable, this kind of a domain wall is highly preferred over the  $\Xi$  states. Static filaments, whose length reaches hundreds  $\mu\text{m}$  [28], are analogous to fixed solitons formed in the one-dimensional system.

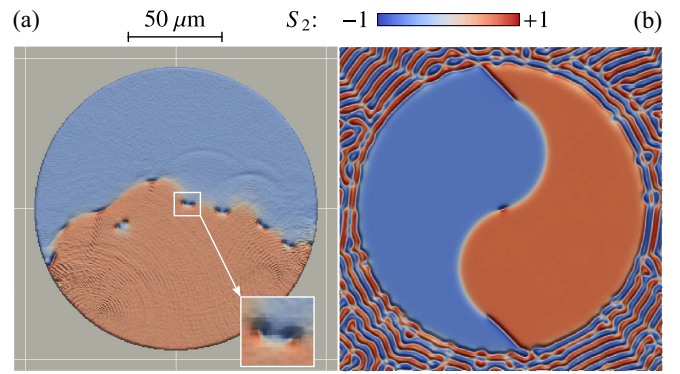


FIG. 4. Snapshots of unsteady solutions of Eq. (1). Parameters  $\gamma$ ,  $g$ , and  $D$  correspond to Fig. 1. The value of  $f^2/f_1^2$  is 6.8 for (a) and 13 for (b). The initial conditions are homogeneous (zero) in both cases. In (a), a very high potential wall is set at  $|\mathbf{r}| = 75 \mu\text{m}$ . In (b),  $\gamma$  is increased from 5 to 200  $\mu\text{eV}$  at the same  $|\mathbf{r}|$ , whereas the boundary conditions are periodic. The obtained pattern steadily rotates clockwise, making a complete turn in 2.6 ns. Supplemental video files explicitly show the evolution of (a) and (b).

Figure 4 illustrates a crossover between single and coupled vortex states, analogous to the transition discovered by Berezinskii, Kosterlitz, and Thouless (BKT) [49,50]. Both patterns [Figs. 4(a) and 4(b)] form spontaneously. In Fig. 4(a), the system is edged by a ring-shaped potential wall similar to Fig. 2. The borderline between the  $\Omega_{\pm}$  domains is of the  $\Xi$  type and moves in space, however, it occasionally slows down and displays vortex filaments. Since  $f$  is not great enough, the filaments break up into the vortex-antivortex dipoles which freely penetrate into the  $\Omega$  domains but have finite lifetime. The whole system evolves irregularly for an indefinite time until it accidentally “finds” a balanced state analogous to Fig. 3 [28].

Instead of setting a potential wall, in Fig. 4(b) we have increased the decay rate  $\gamma$  from 5 to 200  $\mu\text{eV}$  at the same boundary. The pump no longer reaches threshold (6) in the outer area, however, the  $\Sigma_{\pm}$  and  $\Pi$  states are still unstable. Consequently, *all* plane-wave states are forbidden and the system has to be inhomogeneous on the scale  $a \sim k_0^{-1}$ , where  $\hbar^2 k_0^2/2m = D + g/2$  and  $m$  is the polariton mass near  $k = 0$ . In the one-dimensional case, this would have resulted in a stiffly ordered dipolar network [40,46], but the two-dimensional system has more freedom and arranges itself into a labyrinthine structure [45]. It exhibits  $S_2 \sim \pm 1$  at the intensity maxima and  $S_1 = +1$  at the minima and thus can be thought of as a host of vortex filaments in which all vortices are tightly coupled. The inner disk-shaped area contains a single vortex at the center, two curved  $\Xi_+$  and  $\Xi_-$  segments with  $S_1 \sim -1$ , and two straight filaments with  $S_1 \sim +1$  along the core line. This Yin-and-Yang pattern rotates at a fixed angular velocity and represents an instance of unsteady but fully self-consistent polariton states. It was established after  $\sim 9$  ns of irregular evolution when a sole vortex accidentally occurred at the center. More details on the formation of filaments, dipoles, and vortex networks are discussed in the Supplemental Material [28].

In summary, we have found an interesting class of collective bosonic states which arise spontaneously under coherent driving. They are similar to quantized vortices in equilibrium Bose-Einstein condensates and superconductors, featuring a  $2\pi$  phase shift around the core as well as formation of vortex dipoles and filaments in the range of comparatively great driving amplitudes. The character of such a BKT-type crossover suggests the existence of an extremum principle underlying the (de)coupling of vortices, however, it obviously has nothing to do with conventional thermodynamics and calls for further investigation. Solitons and vortices arise

when the spin coupling rate largely exceeds decay rate  $\gamma$ ; nonetheless,  $\gamma$  is nonzero and therefore the field oscillates at the “forced” frequency. As a result, there is no continuous transition to the usual case of freely evolving condensates with  $f = 0$  and  $\gamma = 0$ .

## ACKNOWLEDGMENTS

The work was supported by the Russian Science Foundation (Grant No. 16-12-10538).

- [1] L. Pitaevskii and S. Stringari, *Bose-Einstein Condensation and Superfluidity* (Oxford University Press, New York, 2016).
- [2] A. J. Leggett, *Quantum Liquids: Bose Condensation and Cooper Pairing in Condensed-Matter Systems* (Oxford University Press, New York, 2006).
- [3] G. Blatter, M. V. Feigel'man, V. B. Geshkenbein, A. I. Larkin, and V. M. Vinokur, *Rev. Mod. Phys.* **66**, 1125 (1994).
- [4] M. R. Matthews, B. P. Anderson, P. C. Haljan, D. S. Hall, C. E. Wieman, and E. A. Cornell, *Phys. Rev. Lett.* **83**, 2498 (1999).
- [5] C. N. Weiler, T. W. Neely, D. R. Scherer, A. S. Bradley, M. J. Davis, and B. P. Anderson, *Nature (London)* **455**, 948 (2008).
- [6] J. Scheuer and M. Orenstein, *Science* **285**, 230 (1999).
- [7] K. G. Lagoudakis, M. Wouters, M. Richard, A. Baas, I. Carusotto, R. André, L. S. Dang, and B. Deveaud, *Nat. Phys.* **4**, 706 (2008).
- [8] K. G. Lagoudakis, T. Ostatnický, A. V. Kavokin, Y. G. Rubo, R. André, and B. Deveaud-Plédran, *Science* **326**, 974 (2009).
- [9] Y. Yamamoto, T. Tassone, and H. Cao, *Semiconductor Cavity Quantum Electrodynamics* (Springer, Berlin, 2000).
- [10] A. V. Kavokin, J. J. Baumberg, G. Malpuech, and P. Laussy, *Microcavities*, 2nd ed. (Oxford University Press, New York, 2017).
- [11] J. Kasprzak, M. Richard, S. Kundermann, A. Baas, P. Jeambrun, J. M. J. Keeling, F. M. Marchetti, M. H. Szymanska, R. André, J. L. Staehli, V. Savona, P. B. Littlewood, B. Deveaud, and L. S. Dang, *Nature (London)* **443**, 409 (2006).
- [12] A. Baas, J.-P. Karr, M. Romanelli, A. Bramati, and E. Giacobino, *Phys. Rev. Lett.* **96**, 176401 (2006).
- [13] D. Whittaker, *Superlattices Microstruct.* **41**, 297 (2007).
- [14] F. M. Marchetti, M. H. Szymańska, C. Tejedor, and D. M. Whittaker, *Phys. Rev. Lett.* **105**, 063902 (2010).
- [15] D. N. Krizhanovskii, D. M. Whittaker, R. A. Bradley, K. Guda, D. Sarkar, D. Sanvitto, L. Viña, E. Cerda, P. Santos, K. Biermann, R. Hey, and M. S. Skolnick, *Phys. Rev. Lett.* **104**, 126402 (2010).
- [16] D. Sanvitto, F. M. Marchetti, M. H. Szymanska, G. Tosi, M. Baudisch, F. P. Laussy, D. N. Krizhanovskii, M. S. Skolnick, L. Marrucci, A. Lemaître, J. Bloch, C. Tejedor, and L. Viña, *Nat. Phys.* **6**, 527 (2010).
- [17] D. Sanvitto, S. Pigeon, A. Amo, D. Ballarini, M. De Giorgi, I. Carusotto, R. Hivet, F. Pisanello, V. G. Sala, P. S. S. Guimaraes, R. Houdré, E. Giacobino, C. Ciuti, A. Bramati, and G. Gigli, *Nat. Photonics* **5**, 610 (2011).
- [18] L. Dominici, G. Dagvadorj, J. M. Fellows, D. Ballarini, M. De Giorgi, F. M. Marchetti, B. Piccirillo, L. Marrucci, A. Bramati, G. Gigli, M. H. Szymańska, and D. Sanvitto, *Sci. Adv.* **1**, e1500807 (2015).
- [19] T. Boulier, H. Terças, D. D. Solnyshkov, Q. Glorieux, E. Giacobino, G. Malpuech, and A. Bramati, *Sci. Rep.* **5**, 9230 (2015).
- [20] L. Dominici, R. Carretero-González, A. Gianfrate, J. Cuevas-Maraver, A. S. Rodrigues, D. J. Frantzeskakis, G. Lerario, D. Ballarini, M. De Giorgi, G. Gigli, P. G. Kevrekidis, and D. Sanvitto, *Nat. Commun.* **9**, 1467 (2018).
- [21] T. C. H. Liew, A. V. Kavokin, and I. A. Shelykh, *Phys. Rev. B* **75**, 241301(R) (2007).
- [22] T. C. H. Liew, Y. G. Rubo, and A. V. Kavokin, *Phys. Rev. Lett.* **101**, 187401 (2008).
- [23] S. Pigeon and A. Bramati, *New J. Phys.* **19**, 095004 (2017).
- [24] T. W. Neely, E. C. Samson, A. S. Bradley, M. J. Davis, and B. P. Anderson, *Phys. Rev. Lett.* **104**, 160401 (2010).
- [25] A. Gallemí, L. P. Pitaevskii, S. Stringari, and A. Recati, *Phys. Rev. A* **100**, 023607 (2019).
- [26] K. Ihara and K. Kasamatsu, *Phys. Rev. A* **100**, 013630 (2019).
- [27] Y. G. Rubo, *Phys. Rev. Lett.* **99**, 106401 (2007).
- [28] See Supplemental Material at <http://link.aps.org/supplemental/10.1103/PhysRevB.102.104307> for examples of a system with periodic boundary conditions which allow one to keep the model perfectly uniform and thus explicitly demonstrate the spontaneous character of its instability and secondary ordering, including the BKT-type crossover; besides, separate video files represent the evolution of Figs. 4(a) and 4(b).
- [29] A. V. Sekretenko, S. S. Gavrillov, and V. D. Kulakovskii, *Phys. Rev. B* **88**, 195302 (2013).
- [30] M. Vladimirova, S. Cronenberger, D. Scalbert, K. V. Kavokin, A. Miard, A. Lemaître, J. Bloch, D. Solnyshkov, G. Malpuech, and A. V. Kavokin, *Phys. Rev. B* **82**, 075301 (2010).
- [31] S. Gavrillov, A. Brichkin, A. Dorodnyi, S. Tikhodeev, N. Gippius, and V. Kulakovskii, *JETP Lett.* **92**, 171 (2010).
- [32] P. Stepanov, I. Amelio, J.-G. Rousset, J. Bloch, A. Lemaître, A. Amo, A. Minguzzi, I. Carusotto, and M. Richard, *Nat. Commun.* **10**, 3869 (2019).
- [33] R. Balili, B. Nelsen, D. W. Snoke, R. H. Reid, L. Pfeiffer, and K. West, *Phys. Rev. B* **81**, 125311 (2010).
- [34] S. S. Gavrillov, A. V. Sekretenko, S. I. Novikov, C. Schneider, S. Höfling, M. Kamp, A. Forchel, and V. D. Kulakovskii, *Appl. Phys. Lett.* **102**, 011104 (2013).
- [35] S. S. Gavrillov, A. S. Brichkin, S. I. Novikov, S. Höfling, C. Schneider, M. Kamp, A. Forchel, and V. D. Kulakovskii, *Phys. Rev. B* **90**, 235309 (2014).

- [36] A. V. Sekretenko, S. S. Gavrilov, S. I. Novikov, V. D. Kulakovskii, S. Höfling, C. Schneider, M. Kamp, and A. Forchel, *Phys. Rev. B* **88**, 205302 (2013).
- [37] N. A. Gippius, I. A. Shelykh, D. D. Solnyshkov, S. S. Gavrilov, Y. G. Rubo, A. V. Kavokin, S. G. Tikhodeev, and G. Malpuech, *Phys. Rev. Lett.* **98**, 236401 (2007).
- [38] V. F. Elesin and Y. V. Kopaev, *Zh. Eksp. Teor. Fiz.* **63**, 1447 (1972) [*Sov. Phys. JETP* **36**, 767 (1973)].
- [39] A. Baas, J. P. Karr, H. Eleuch, and E. Giacobino, *Phys. Rev. A* **69**, 023809 (2004).
- [40] S. S. Gavrilov, *Phys. Usp.* **63**, 123 (2020).
- [41] S. S. Gavrilov, A. A. Demenev, and V. D. Kulakovskii, *JETP Lett.* **100**, 817 (2015).
- [42] S. S. Gavrilov and V. D. Kulakovskii, *JETP Lett.* **104**, 827 (2016).
- [43] I. A. Shelykh, D. D. Solnyshkov, G. Pavlovic, and G. Malpuech, *Phys. Rev. B* **78**, 041302(R) (2008).
- [44] S. S. Gavrilov, *JETP Lett.* **105**, 200 (2017).
- [45] S. S. Gavrilov, *Phys. Rev. B* **94**, 195310 (2016).
- [46] S. S. Gavrilov, *Phys. Rev. Lett.* **120**, 033901 (2018).
- [47] C. E. Whittaker, B. Dzurak, O. A. Egorov, G. Buonaiuto, P. M. Walker, E. Cancellieri, D. M. Whittaker, E. Clarke, S. S. Gavrilov, M. S. Skolnick, and D. N. Krizhanovskii, *Phys. Rev. X* **7**, 031033 (2017).
- [48] G. Díaz-Camacho, C. Tejedor, and F. M. Marchetti, *Phys. Rev. B* **97**, 245309 (2018).
- [49] J. M. Kosterlitz and D. J. Thouless, *J. Phys. C* **6**, 1181 (1973).
- [50] Z. Hadzibabic, P. Krüger, M. Cheneau, B. Battelier, and J. Dalibard, *Nature (London)* **441**, 1118 (2006).